Nonglutamate Pore Residues in Ion Selection and Conduction in Voltage-Gated Ca^{2+} Channels

Anna V. Williamson and William A. Sather
Department of Pharmacology and Program in Neuroscience, University of Colorado Health Sciences Center, Denver, Colorado 80262 USA

ABSTRACT High-affinity, intrapore binding of Ca^{2+} over competing ions is the essential feature in the ion selectivity mechanism of voltage-gated Ca^{2+} channels. At the same time, several million Ca^{2+} ions can travel each second through the pore of a single open Ca^{2+} channel. How such high Ca^{2+} flux is achieved in the face of tight Ca^{2+} binding is a current area of inquiry, particularly from a structural point of view. The ion selectivity locus comprises four glutamate residues within the channel's pore. These glutamates make unequal contributions to Ca^{2+} binding, underscoring a role for neighboring residues in pore function. By comparing two Ca^{2+} channels (the L-type α_{1C}, and the non-L-type α_{1A}) that differ in their pore properties but only differ at a single amino acid position near the selectivity locus, we have identified the amino-terminal neighbor of the glutamate residue in motif III as a determinant of pore function. This position is more important in the function of α_{1C} channels than in α_{1A} channels. For a systematic series of mutations at this pore position in α_{1C}, both unitary Ba^{2+} conductance and Cd^{2+} block of Ba^{2+} current varied with residue volume. Pore mutations designed to make α_{1C} more like α_{1A} and vice versa revealed that relative selectivity for Ba^{2+} over K^+ depended almost solely on pore sequence and not channel type. Analysis of thermodynamic mutant cycles indicates that the motif III neighbor normally interacts in a cooperative fashion with the locus, molding the functional behavior of the pore.

INTRODUCTION

Ca^{2+} flow through voltage-gated Ca^{2+} channels occurs at a rate of $\sim 10^6$ ions/s, with an error rate of only ~ 1 ion in 10^4 (Lansman et al., 1986; Hess et al., 1986; Hess and Tsien, 1984; Almers and McCleskey, 1984). Such high-fidelity, high-throughput Ca^{2+} channel performance is important in a wide range of excitable cell function, from very fast events such as neurotransmitter release, to slower ones such as the heart beat, and to slower ones still, such as regulation of gene expression. As a consequence of both this physiological significance and remarkable functional performance, the physical mechanism and pore structure that support Ca^{2+} flow through voltage-gated Ca^{2+} channels have been in the spotlight of biophysical research (McCleskey, 1999).

Ion selectivity of Ca^{2+} channels is founded upon the large difference in pore-binding affinity between Ca^{2+} and Na^+ ions: a single Ca^{2+} ion binds $>10^3$-fold tighter, or longer, than does a Na^+ ion. Fast Ca^{2+} flux through Ca^{2+} channels, on the other hand, relies upon a negative interaction between Ca^{2+} ions within the pore to overcome the otherwise too-tight binding of a single Ca^{2+} ion; the physical nature of this negative interaction is perhaps part competition for liganding groups involved in ion binding and part electrostatic repulsion between ions (Hess and Tsien, 1984; Almers and McCleskey, 1984; Almers et al., 1984; Kostyuk et al., 1983). The binding of Ca^{2+} is carried out by a cluster of four glutamate residues located in the channel's pore lining (Kim et al., 1993), which is itself contained within the single pore-forming α_1 subunit (Tang et al., 1993; Yang et al., 1993). This subunit consists of four homologous domains, or motifs, which are believed to be arranged around the central, ion-conducting pore in such a way that each quadrant in the cross section of the α_1 subunit is occupied by one motif. Each motif possesses a pore-lining sequence, the P-loop, that bears one of the four Ca^{2+}-binding glutamate (E) residues that are collectively referred to as the EEEE locus. An alternative view is that Ca^{2+} channels lack a discrete high-affinity binding locus and that instead the electrostatic potential profile within the channel's pore favors the flux of Ca^{2+} over that of Na^+ (Nonner and Eisenberg, 1998). Although this Poisson-Nernst-Planck model has many attractive features, it is not reconcilable with the extensive results of EEEE locus mutagenesis and is therefore not considered further here (see McCleskey, 1999).

Site-directed mutagenesis in the EEEE locus has demonstrated its essential role in selective ion permeation in Ca^{2+} channels (Ellinor et al., 1995; Yang et al., 1993). One of the conclusions drawn from that work was that the EEEE locus is structurally flexible; it is able to bind a single Ca^{2+} ion with high affinity ($K'_D \sim 1$ μM) or rearrange to bind a pair of Ca^{2+} ions with much lower affinity ($K'_D \sim 14$ mM) (Yang et al., 1993). Thus the current view of selective Ca^{2+} flux combines this structural information with the earlier, binding-based models: high-affinity EEEE locus binding of a single Ca^{2+} ion forms the basis of selectivity for Ca^{2+} over Na^+, while lowered affinity of Ca^{2+} binding in the doubly occupied state of the EEEE locus permits fast Ca^{2+} flux. The mutagenesis results also demonstrated that the

Received for publication 9 June 1999 and in final form 26 July 1999.

Address reprint requests to Dr. William A. Sather, Neuroscience Center, Box B-138, University of Colorado Health Sciences Center, 4200 East Ninth Avenue, Denver, CO 80262. Tel.: 303-315-3986; Fax: 303-315-3431; E-mail: william.sather@uchsc.edu.

© 1999 by the Biophysical Society

0006-3495/99/11/2575/15 $2.00

EEEE locus glutamates make nonequivalent contributions to Ca^{2+} binding (Bahinski et al., 1997; Ellinor et al., 1995; Parent and Gopalakrishnan, 1995; Yatani et al., 1994a; Mikala et al., 1993; Kim et al., 1993; Yang et al., 1993), suggesting that they form a functionally asymmetrical binding site.

Does functional asymmetry within the EEEE locus hint at distinct functional roles for individual glutamates? Specifically, might nonequivalence between EEEE locus glutamates reflect the specialization of individual glutamates to support fast Ca^{2+} flux? In this scenario, some glutamates are preferentially involved in facilitating external Ca^{2+} entry into the locus, while others are preferentially involved in facilitating the departure of EEEE locus Ca^{2+} to the cytosol. Based on this speculation, investigation of the structural origins of glutamate nonequivalence represents an effort to elucidate the structural requirements for rapid flux through the selectivity locus.

Functional asymmetry of the EEEE locus must arise in some manner from the structure of the protein, with critical residues that confer specialized, motif-dependent glutamate functionality likely lying in close proximity to the EEEE locus. Neighboring residues are envisioned as influencing Ca^{2+} binding within the pore in one or more of three ways: 1) via steric action to determine spatial positioning of the EEEE locus glutamates; 2) via electrostatic interaction to modify the electronegativity, or pK_a, of the EEEE locus carboxylate groups; or 3) via direct contribution to the binding of permeating ions. In the absence of a high-resolution structure for Ca^{2+} channels, EEEE locus neighbors, with the exception of near neighbors in the amino acid sequence, remain unidentified. Focusing therefore upon these known sequence neighbors, various comparative mutagenesis strategies may be used to tease out potential effects of these amino acids upon EEEE locus function. One straightforward strategy involves swapping neighbor amino acids between motifs of a Ca^{2+} channel. An alternative strategy is to compare two different kinds of Ca^{2+} channels, testing whether differences in channel properties (binding affinity, conductance) correlate with differences in neighbor identity. We have pursued the latter strategy as our first step because there are fewer differences in the identity of sequence neighbors when comparing, for any given motif, across channel types than there are when comparing across motifs for any given channel (Table 1). We specifically compared α_{1C} and α_{1A} channels, which share only ~40% amino acid sequence identity, for the following reasons: first, there is a robust, twofold difference between them in single-channel conductance, and second, there is a 20-fold difference between them in the effect on divalent cation binding affinity of glutamine substitution for the motif III glutamate (Kim et al., 1993; Yang et al., 1993). Considering two neighbors on either side of each of the four EEEE locus glutamates, or 16 neighbors for each of the channels, wild-type α_{1C} and α_{1A} channels differ from one another at only a single position: on the amino-terminal side of the glutamate residue in motif III, a phenylalanine is present in α_{1C}, whereas a glycine is present in α_{1A} (Table 1, *boxed residues*). Using site-directed mutagenesis, we have found that the nature of the amino acid at this key position is a determining factor in the single-channel conductance of α_{1C} channels but is less important in α_{1A} channels. We have also found for both α_{1C} and α_{1A} channels, using mutant cycle analysis, that the amino acid located at this position interacts with the EEEE locus glutamate in motif III during the binding of divalent cations.

MATERIALS AND METHODS

Construction of Ca^{2+} channel mutants

To enhance expression of α_{1C} (rabbit cardiac Ca^{2+} channel α_1 subunit, pCARD3; Mikami et al., 1989) in *Xenopus* oocytes the α_{1C} insert lacking the upstream untranslated region was subcloned into a modified version of the pGEM-3Z vector bearing the 5′ and 3′ untranslated regions of the *Xenopus* β-globin gene (Liman et al., 1992). In addition, a consensus Kozak sequence for the initiation of protein synthesis was incorporated immediately adjacent to the start methionine, and the resulting recombinant plasmid was termed pCARDHE. Site-directed point mutations in motif III of α_{1C} and α_{1A} (rabbit brain Ca^{2+} channel BI-2; Mori et al., 1991) were created using a megaprimer polymerase chain reaction-based method. The mutant cassettes were ligated into the full-length cDNA between the unique restriction enzyme sites *Sal*I (3435) and *Sna*BI (3836) in α_{1C} or *Nhe*I (3543) and *Acc*I (4799) in α_{1A}. DNA sequences of mutant constructs were confirmed using diagnostic restriction enzyme digests and dideoxy chain termination sequencing of the entire polymerase chain reaction cassette.

Ca^{2+} channel expression in *Xenopus* oocytes

Female *Xenopus laevis* were anesthetized by a ~30-min immersion in a 0.2% tricaine methanesulfonate solution, ovarian tissue was removed via an abdominal incision, and the incision was then sutured. Individual

TABLE 1 Alignment of pore sequences for high voltage-activated Ca^{2+} channels

	Motif *I*					Motif *II*					Motif *III*					Motif *IV*				
	−2	*−1*	*0*	*1*	*2*	*−2*	*−1*	*0*	*1*	*2*	*−2*	*−1*	*0*	*1*	*2*	*−2*	*−1*	*0*	*1*	*2*
α_{1C}	T	M	E	G	W	T	G	E	D	W	T	F	E	G	W	T	G	E	A	W
α_{1D}	T	M	E	G	W	T	G	E	D	W	T	F	E	G	W	T	G	E	A	W
α_{1S}	T	M	E	G	W	T	G	E	D	W	T	F	E	G	W	T	G	E	A	W
α_{1A}	T	M	E	G	W	T	G	E	D	W	T	G	E	G	W	T	G	E	A	W
α_{1B}	T	M	E	G	W	T	G	E	D	W	T	G	E	G	W	T	G	E	A	W
α_{1E}	T	M	E	G	W	T	G	E	D	W	T	G	E	G	W	T	G	E	A	W

EEEE locus glutamates are located at position 0 in each motif.

oocytes were dissociated from ovarian tissue by agitation for 90 min in Ca^{2+}-free OR-2 solution (in mM: 82.5 NaCl, 2 KCl, 1 $MgCl_2$, 5 HEPES, pH 7.5 with NaOH) containing 2 mg/ml collagenase B (Boehringer-Mannheim, Indianapolis, IN). The oocytes were rinsed in fresh OR-2 solution, and stage V and VI oocytes were selected by hand. cRNAs encoding wild-type and mutant forms of α_{1C}, α_{1A}, β_{2b} (pBH17; Hullin et al., 1992), and $\alpha_2\delta$ (pCA1S; Mikami et al., 1989) were synthesized by in vitro transcription. A 1:1:1 molar ratio mix of α_1, β_{2b}, and $\alpha_2\delta$ was injected into oocytes. Injected oocytes were incubated at 18°C for up to 2 weeks in ND96 solution (in mM: 96 NaCl, 2 KCl, 1.8 $CaCl_2$, 1 $MgCl_2$, 5 HEPES, pH 7.6 with NaOH) supplemented with 2.5 mM sodium pyruvate and a mix of 100 units/ml penicillin plus 0.1 mg/ml streptomycin (Sigma, St. Louis, MO).

Two-electrode voltage-clamp recording

Whole-oocyte membrane currents were recorded using a two-electrode voltage-clamp amplifier (OC-725B; Warner Instruments, Hamden, CT), and currents were filtered at 1 kHz (−3 dB; 4-pole Bessel filter) and sampled at 2 kHz. Currents were evoked every 15 s by 150 ms step depolarizations from a holding potential of −80 mV. When Cd^{2+} dose-inhibition data were collected, step depolarizations to +20 mV were used. Leak and capacity currents were subtracted, using the average of 10 $-P/4$ pulses, where P was the test pulse amplitude. Dose-inhibition functions were calculated according to a 1:1 binding relationship: $I/I_{con} = 1/(1 + [Cd^{2+}]/IC_{50})$, where I is current in the test condition, I_{con} is control current in the absence of Cd^{2+}, $[Cd^{2+}]$ is the concentration of the blocking ion, and IC_{50} is the half-block concentration. Conductance-voltage data were fit with Boltzmann functions of the form $g/g_{max} = [1 + \exp((V_{0.5} - V_M)/b)]^{-1}$, where g/g_{max} is the normalized peak chord conductance, $V_{0.5}$ is the half-activation voltage, V_M is the membrane potential, and b is the Boltzmann slope parameter.

During recording, solutions were gravity fed (~1 ml/min) into one end of a flow-through perfusion chamber and were removed via suction at the opposite end. Solutions were exchanged by switching between reservoirs containing different solutions. Pipettes were filled with 3 M KCl and typically had a resistance of 1.5–3 MΩ. For most recordings oocytes were bathed in a standard Cl^--free Ba^{2+} solution of the following composition (in mM): (nominally) 40 $Ba(OH)_2$, 52 tetraethylammonium hydroxide (TEA-OH), 5 HEPES (pH 7.4 with methane sulfonic acid (CH_4SO_3)). The addition of methane sulfonic acid produced a Ba^{2+} precipitate, which was removed by filtration. Chemical analysis of the filtered solution (Evergreen Analytical, Wheat Ridge, CO) revealed that the Ba^{2+} concentration ranged from 8.7 to 11.7 mM and averaged ~10 mM; in keeping with the extensive body of previous work utilizing this solution, however, we have continued to refer to this solution as 40 mM Ba^{2+}.

For Cd^{2+} block of Ba^{2+} experiments, $CdCl_2$ stock solutions were diluted in the standard Ba^{2+} solution to the desired final Cd^{2+} concentration.

Single-channel recording

After oocytes were soaked in a hyperosmotic solution for several minutes, the vitelline membrane was stripped away with fine forceps. Stripped oocytes were placed in 35-mm culture dishes containing a high K^+ solution (in mM: 100 KCl, 10 HEPES, 10 EGTA, pH 7.4 with KOH) that zeroed the membrane potential during cell-attached patch recording, and recordings were carried out on the stage of an inverted microscope. Patch pipettes were coated with Sylgard (Dow Corning, Midland, MI), fire polished, and filled with a solution containing (in mM) 110 $BaCl_2$, 10 HEPES (pH 7.4 with TEA-OH). Typical patch pipette resistances were in the range of 18–25 MΩ. Single-channel currents were recorded using an Axopatch 200B patch-clamp amplifier (Axon Instruments, Foster City, CA), filtered at 2 kHz (−3 dB; 8-pole Bessel filter, Frequency Devices, Haverhill, MA), and sampled at 10 kHz. Voltage steps from a holding potential of −80 mV were applied at 3 s intervals, and the test potential duration was 300 ms.

Data were collected using Pulse software (Heka, Instrutech, Great Neck, NY) and analyzed using a combination of Pulse and Tac/TacFit (Bruxton Corporation, Seattle, WA). Single-channel current amplitudes were readily determined by simple cursor analysis for wild-type and mutant α_{1C} channels because channel open time was in the range of 10–50 ms, owing to the action of FPL 64176 (2 μM bath concentration; RBI, Natick, MA). For wild-type and mutant α_{1A} channels (which are insensitive to FPL 64176), either all-points histograms or amplitude histograms for >300 individual open channel events were constructed and fit with single Gaussian functions to obtain the mean and standard deviation of the amplitude distributions.

Calculation of free energy of Ca^{2+} binding and permeability ratios

The Gibbs free energy (ΔG) of Cd^{2+} bound within the channel pore was calculated for wild-type and mutant channels with the following equation:

$$\Delta G = (k_B T)\ln(K'_D) \quad (1)$$

where k_B is Boltzmann's constant, T is absolute temperature (Kelvin), and K'_D (molar) is the apparent dissociation constant for Cd^{2+}. K'_D is taken as the concentration of Cd^{2+} that produces half-block of the whole-cell Ba^{2+} current (IC_{50}).

The permeability of external Ba^{2+} relative to internal K^+ (P_{Ba}/P_K) was calculated for wild-type and mutant channels, using a form of the Goldman-Hodgkin-Katz voltage equation modified for the case in which the permeant ion species differ in valence. The specific form of the equation was adapted from Eq. 7 in Campbell et al. (1988). Neglecting terms for extracellular K^+ ($[K^+]_o$), because this was 0, and intracellular Ba^{2+} ($[Ba^{2+}]_i$), because this was small and unknown, and employing ion activities in place of concentrations, the final equation is

$$P_{Ba}/P_K = \left(\frac{y_K[K^+]_i}{4y_{Ba}[Ba^{2+}]_o}\right)(\exp(2E_{rev}F/RT) + \exp(E_{rev}F/RT)) \quad (2)$$

where $[K^+]_i$ and $[Ba^{2+}]_o$ are intracellular K^+ and extracellular Ba^{2+} concentrations, y_K and y_{Ba} are the activity coefficients for K^+ and Ba^{2+} (molar scale), E_{rev} is the measured reversal potential, F is Faraday's constant, R is the gas constant, and T is temperature (Kelvin). Using an ion-selective microelectrode, the intracellular activity of K^+ ($y_K \cdot [K^+]_i$) in stage V–VI *Xenopus* oocytes has been measured directly as 92.5 mM (Barrish, 1983). Lacking a similar measurement for the activity of Ba^{2+} ions in our external solution, we calculated this quantity using the Guggenheim extension of the Debye-Hückel limiting law for ions in aqueous solution. However, this equation yields the mean activity coefficient for dissolved cation-anion pairs. To determine the activity coefficient for Ba^{2+} alone (y_{Ba}), we followed the Guggenheim convention for the calculation of single-ion activity coefficients from mean activity coefficients (where $y_{Ba(CH4SO3)2}$ = mean activity coefficient for Ba^{2+}-methanesulfonate; see Eqs. 1–4 in Blinks et al. (1982)): $y_{Ba} = y^2_{Ba(CH4SO3)2}$. The final formulation of the equation used to calculate y_{Ba} was

$$y_{Ba} = 10\exp\{2[(|z_+z_-|\sigma/10) - (A|z_+z_-|\sqrt{\sigma}/1 + \sigma^{1/2})]\} \quad (3)$$

where σ is the ionic strength of the solution in molarity, A is an empirical constant with a value of 0.51 at 25°C (Robinson and Stokes, 1959), and z_+ ($Ba^{2+} = +2$) and z_- (methanesulfonate = −1) are the valences of the cation/anion pair of interest. Ionic strength was calculated as

$$\sigma = \frac{1}{2}\sum_{j=1}^{n} c_j z_j^2 \quad (4)$$

where c_j and z_j are the concentration (molar) and valence of the jth ion species in the solution. In calculating P_{Ba}/P_K, we used the average mea-

sured Ba^{2+} concentration (10 mM) in the nominally 40 mM Ba^{2+} solution. The calculated ionic strength of the 40 mM Ba^{2+} solution was 0.085, and y_{Ba} was 0.373.

All experiments were carried out at room temperature (~22°C). All numerical values are given as mean ± SEM unless otherwise specified.

Nomenclature

Because the only structural differences between the channels studied were in α_1 subunits, for brevity, all channels are referred to here only by a specific α_1 subunit name. The previously identified four glutamate residues that are essential for normal ion selectivity in wild-type Ca^{2+} channels are referred to, in ensemble, as the EEEE locus. Individually, they are designated E_I, E_{II}, E_{III}, and E_{IV}, with the Roman numeral subscripts indicating the motif of origin of each glutamate. Also for brevity, the EEEE locus glutamates are numbered "0" in each motif, neighbors to the amino-terminal side of the glutamates are assigned negative position numbers (−1 for the immediate amino-terminal neighbor, −2 for the next closest neighbor to the amino terminal side), and the neighbors to the carboxy terminal side are assigned positive position numbers. As this paper concerns motif III mutations only (substitution of the glutamate residue, of the amino acids at the −1 position, or of both the glutamate and the −1 neighbor), wild-type channels are referred to as α_{1C}^{FEG} and α_{1A}^{GEG}. Mutated residues are marked in bold and underlined: as examples, the F→G switch in α_{1C} is referred to as α_{1C}^{GEG}, and the G→F switch in α_{1A} is referred to as α_{1A}^{FEG}. Glutamine (Q) substitutions at E_{III} in α_{1C} or α_{1A} are referred to as $E_{III}Q$ mutations. The $E_{III}Q$ mutation in a specific α_1 subunit type is referred to as α_{1C}^{FQG} or α_{1A}^{GQG}. (In the one-letter code, A = alanine, E = glutamate, F = phenylalanine, G = glycine, L = leucine, M = methionine, Q = glutamine, V = valine, and Y = tyrosine.)

RESULTS

Effects of single mutations at the −1 neighbor position

As illustrated in Table 1, threonine, glutamate, and tryptophan residues occupy the −2, 0, and +2 positions in all four motifs of every high-voltage activated Ca^{2+} channel. There are, in contrast, many differences between the motifs at both the −1 and +1 positions. However, when comparing a given motif with its counterparts in other channels, that is, when comparing first motifs with first motifs and second motifs with second motifs and so on, there is only a single nonconserved −1 or +1 neighbor: all three L-type Ca^{2+} channels (α_{1C}, α_{1D}, α_{1S}) possess a phenylalanine residue at the −1 position in motif III, whereas the non-L channels (α_{1A}, α_{1B}, α_{1E}) possess a glycine residue at this position (Table 1, *boxed residues*). Focusing specifically upon comparison of α_{1C} and α_{1A} as examplar subtypes, we have combined site-directed mutagenesis and electrophysiological measurement to examine the potential of this sole divergence in near-EEEE locus sequence to determine subtype-specific pore function.

Wild-type and mutant Ca^{2+} channels were expressed in *Xenopus* oocytes, and whole-oocyte Ba^{2+} currents carried by these channels were measured using two-electrode voltage clamp. Fig. 1 presents families of current records and current-voltage data for wild-type α_{1C} and α_{1A} channels and for −1 position mutants of α_{1C} (F→G; α_{1C}^{GEG}) and of α_{1A} (G→F; α_{1A}^{FEG}). As illustrated in the figure, mutations at the −1 position did not significantly alter the voltage-dependent kinetics of activation or inactivation of α_{1C} or α_{1A} channels. Channel selectivity for Ba^{2+} over K^+ was also unaltered by −1 position mutations, as evidenced by the unchanged reversal potentials (~70 mV for both α_{1C} and α_{1A}).

The −1 position determines single-channel conductance in α_{1C} but not in α_{1A}

In contrast to the absence of effect of the −1 position mutation on channel kinetics and reversal potential, single-channel conductance was influenced by −1 position mutation, particularly for the α_{1C} channel. Single-channel currents were recorded from cell-attached patches on *Xenopus* oocytes, with 110 mM Ba^{2+} in the patch pipette. Fig. 2 shows the influence on unitary current amplitude of the F→G mutation in α_{1C} and the G→F mutation in α_{1A}. In α_{1C} channels, the glycine substitution greatly reduced unitary current amplitude at 0 mV, as shown in Fig. 2 *A* (*top*). The wild-type channel (α_{1C}^{FEG}) had an average unitary current amplitude of 1.2 ± 0.1 pA ($n = 6$) at 0 mV, whereas the mutant α_{1C}^{GEG} had a much smaller amplitude of 0.3 ± 0.1 pA ($n = 3$) at 0 mV. On the other hand, phenylalanine substitution in α_{1A} had little effect on unitary current (Fig. 2 *B*, *top*). Mean unitary current amplitudes at 0 mV were 0.9 ± 0.1 pA ($n = 4$) for α_{1A}^{GEG} (WT) and 0.7 ± 0.1 pA ($n = 4$) for α_{1A}^{FEG}. Note that the obvious difference in open time between α_{1C} and α_{1A} channels was due to the result of FPL 64176 action on α_{1C} channels: this benzoyl pyrrole prolongs the open time of L-type Ca^{2+} channels, such as α_{1C}, from ~1 ms to ~10–50 ms (see Materials and Methods). FPL 64176 was used simply to facilitate measurement of single-channel current amplitude for α_{1C} channels, does not itself affect current amplitude, and was not used in experiments with α_{1A} channels because they are insensitive to the compound.

Single-channel current-voltage relationships for wild-type and mutant α_{1C} and α_{1A} channels are illustrated in the bottom panels of Fig. 2, *A* and *B*, respectively. At all test potentials, the amplitudes of the currents through the mutant α_{1C}^{GEG} channel were much smaller than those through the wild-type α_{1C}^{FEG} channel and yielded a unitary slope conductance of 13 pS for the mutant compared to 30 pS for wild type. Similar analysis of mutant and wild-type α_{1A} currents showed that currents through mutant α_{1A}^{FEG} channels were somewhat smaller than those through wild-type α_{1A} channels, and the corresponding slope conductances were 13 pS for the mutant and 17 pS for wild type. Despite the brevity of mutant and wild-type α_{1A} open times, the amplitudes were well resolved, as shown by the example amplitude histograms (0 mV) and fitted Gaussian distributions in Fig. 2 *C*.

The −1 position in α_{1C} and single-channel conductance

Although F→G substitution at the −1 position in α_{1C} significantly diminished single-channel conductance, the reciprocal mutation in α_{1A} had little such effect, indicating

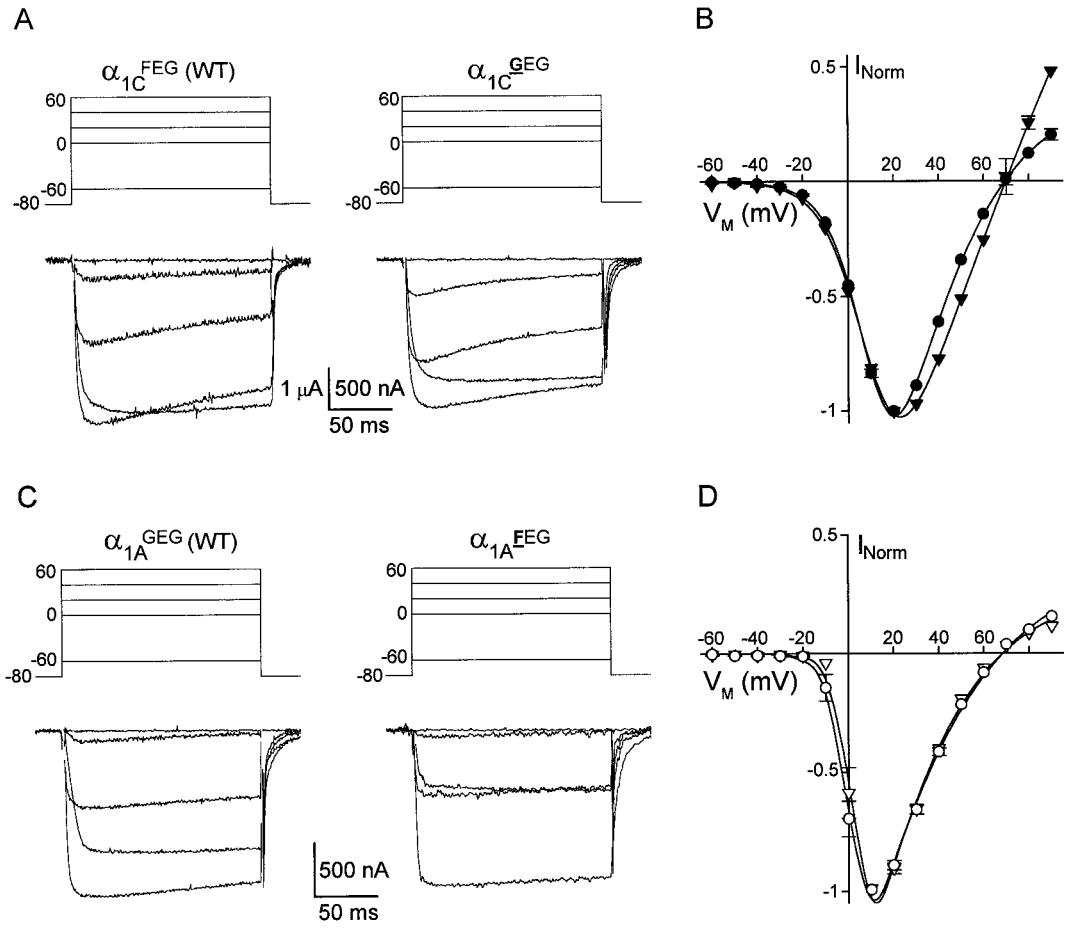

FIGURE 1 Ba^{2+} current records and current-voltage relationships from whole-oocyte recordings of wild-type and −1 position mutant channels. (*A*) Families of whole-oocyte Ba^{2+} currents carried by the wild-type α_{1C}^{FEG} channel and the mutant α_{1C}^{GEG} channel. Current records illustrated were obtained at −60, 0, +20, +40, and +60 mV. Holding potential, −80 mV; 40 mM Ba^{2+} external solution. (*B*) Normalized current-voltage relationships (obtained by normalizing peak current-voltage relationships from individual cells to the maximum inward current observed in the test potential range −60 to +90 mV) for the wild-type α_{1C}^{FEG} channel (●; $n = 4$) and the mutant α_{1C}^{GEG} channel (▼; $n = 6$). Holding potential, −80 mV; 40 mM Ba^{2+} external solution. (*C*) Families of whole-oocyte Ba^{2+} currents carried by the wild-type α_{1A}^{GEG} channel and the mutant α_{1A}^{FEG} channel. Current records illustrated were obtained at −60, 0, +20, +40, and +60 mV. Holding potential, −80 mV; 40 mM Ba^{2+} external solution. (*D*) Normalized current-voltage relationships for the wild-type α_{1A}^{GEG} channel (○; $n = 7$) and the mutant α_{1A}^{FEG} channel (▽; $n = 7$).

that this particular pore lining position is not in itself responsible for the difference in unitary conductance between these two kinds of Ca^{2+} channels. Nevertheless, the profound effect of the glycine substitution in α_{1C} suggested that the −1 position in this channel is important in determining unitary conductance. To pursue this idea, we constructed a series of −1 position α_{1C} mutants, guided by distinctions between phenylalanine and glycine in steric and chemical properties: phenylalanine possesses a bulky aromatic side chain, whereas glycine has the smallest side chain of all of the natural amino acids, a single hydrogen atom. In place of the wild-type phenylalanine residue at the −1 position in α_{1C}, we substituted the bulky aromatic tyrosine (α_{1C}^{YEG}), and a series of progressively smaller hydrophobic amino acids: leucine (α_{1C}^{LEG}), methionine (α_{1C}^{MEG}), valine (α_{1C}^{VEG}), and alanine (α_{1C}^{AEG}). Fig. 3 *A* illustrates single-channel current records at −40 mV for these mutants and the wild-type α_{1C} channel. The α_{1C}^{YEG} mutant was virtually identical to wild type in unitary current amplitude, but current amplitude decreased progressively over the series α_{1C}^{LEG}, α_{1C}^{MEG}, α_{1C}^{VEG}, α_{1C}^{AEG}, and α_{1C}^{GEG}. Fig. 3 *B* compares mean unitary current-voltage relationships for wild-type and mutant channels, showing that single-channel conductance also decreases over this series of constructs, in register with their progressively decreasing side-chain volume. Fig. 3 *C* illustrates this trend, plotting unitary conductance versus residue volume. Single-channel conductance in α_{1C} appears to be highly dependent upon residue volume at the −1 position in the P-loop of motif III.

The −1 position in α_{1C} and ion selectivity: reversal potential

Because the −1 position mutants in α_{1C} altered the conductance of Ba^{2+} ions through the pore, a natural question is whether these mutants also alter the selective preference of

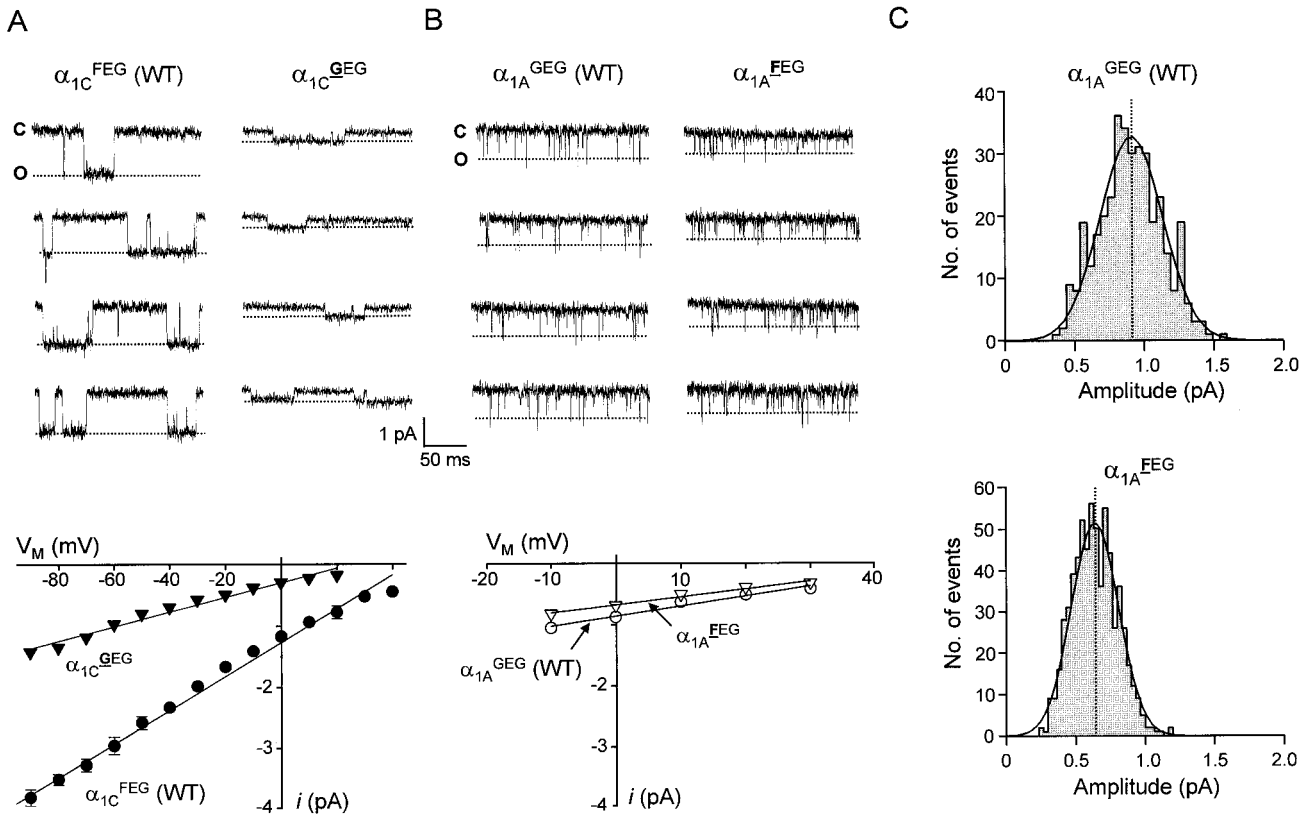

FIGURE 2 Single-channel current-voltage relationships for $\alpha_{1C}{}^{FEG}$ (WT), $\alpha_{1A}{}^{GEG}$ (WT), and the -1 position mutants $\alpha_{1C}{}^{GEG}$ and $\alpha_{1A}{}^{FEG}$. (*A*) Single-channel current records and current-voltage plots for wild-type $\alpha_{1C}{}^{FEG}$ (●; $n = 3$–6) and the mutant channel $\alpha_{1C}{}^{GEG}$ (▼; $n = 3$–5). Inward currents were carried by 110 mM Ba^{2+}. FPL 64176 (2 μM) was present in the bath to prolong the channel open time. Holding potential, -80 mV; test potential, 0 mV. Dotted lines indicate the full open amplitude. c = closed, o = open. (*B*) Single-channel records (110 mM Ba^{2+}) and current-voltage plots for wild-type channel $\alpha_{1A}{}^{GEG}$ (○; $n = 3$–5) and $\alpha_{1A}{}^{FEG}$ (▽; $n = 3$–8). FPL 64176 was not included in the bath in these experiments because α_{1A} channels are insensitive to this compound. Holding potential, -80 mV; test potential, 0 mV. Dotted lines indicate the full open amplitude. (*C*) Amplitude histograms for (*top*) wild-type $\alpha_{1A}{}^{GEG}$ and (*bottom*) $\alpha_{1A}{}^{FEG}$ channels, constructed from >300 individual openings at a test potential of 0 mV and in 110 mM Ba^{2+}. Superimposed smooth curves represent fitted Gaussian distributions. Dotted vertical lines indicate mean open-channel amplitudes from the fits.

the α_{1C} channel for Ba^{2+}, as revealed by reversal potential measurements for whole-oocyte currents. The -1 position mutations ($\alpha_{1C}{}^{YEG}$, $\alpha_{1C}{}^{LEG}$, $\alpha_{1C}{}^{MEG}$, $\alpha_{1C}{}^{VEG}$, $\alpha_{1C}{}^{AEG}$, and $\alpha_{1C}{}^{GEG}$) did not grossly alter whole-oocyte current waveforms as compared to wild-type α_{1C} (data not shown). Whole-oocyte current-voltage data for the -1 position mutants are superimposed on the wild-type data in Fig. 4 *A*, showing that the shapes of the current-voltage relationships for the mutants differed only modestly from that of wild type (*filled circles*). These shape differences corresponded largely to mild differences in the voltage dependence of channel activation: fits of Boltzmann functions to conductance-voltage transforms of the current-voltage data yielded half-activation voltages for the mutants of $V_{0.5} = -2.8$ to $+9.4$ mV and Boltzmann slope factors of $b = 6.5$ to -9.3 mV, compared to wild-type values of $V_{0.5} = +5.5$ and $b = 6.5$. Most pertinent to our focus on selective ion permeability, however, the reversal potential values for the mutants were not different from that of wild-type (Fig. 4 *B*), showing that the -1 position mutations did not measurably alter the channel's preference for external Ba^{2+} over internal K^+.

It is noteworthy that the $\alpha_{1C}{}^{GEG}$ and $\alpha_{1C}{}^{AEG}$ mutants (*filled triangles* and *empty diamonds* in Fig. 4 *A*), which bear the smallest van der Waals volume substitutions at the -1 position, exhibited the largest outward currents. Large outward currents were not present in uninjected oocytes, were appropriately blocked by the L-type Ca^{2+} channel blocker Cd^{2+}, and were carried by K^+ ions exiting the oocyte through the heterologously expressed Ca^{2+} channels. That these two mutants differed little from wild type in voltage-dependent kinetics of activation and inactivation suggests that outward conduction of K^+ was significantly altered with either alanine or glycine substituted at the -1 position. The next smallest substitution at the -1 position, valine (Fig. 4 *A*, *open squares*), was correlated with the next largest outward currents, with substitutions by larger volume amino acids at this position either not changing or slightly reducing outward K^+ current. These results are consistent with a trend of enhanced K^+ conduction for decreased volume at the -1 position, even though none of the substitutions measurably altered selectivity for Ba^{2+} over K^+.

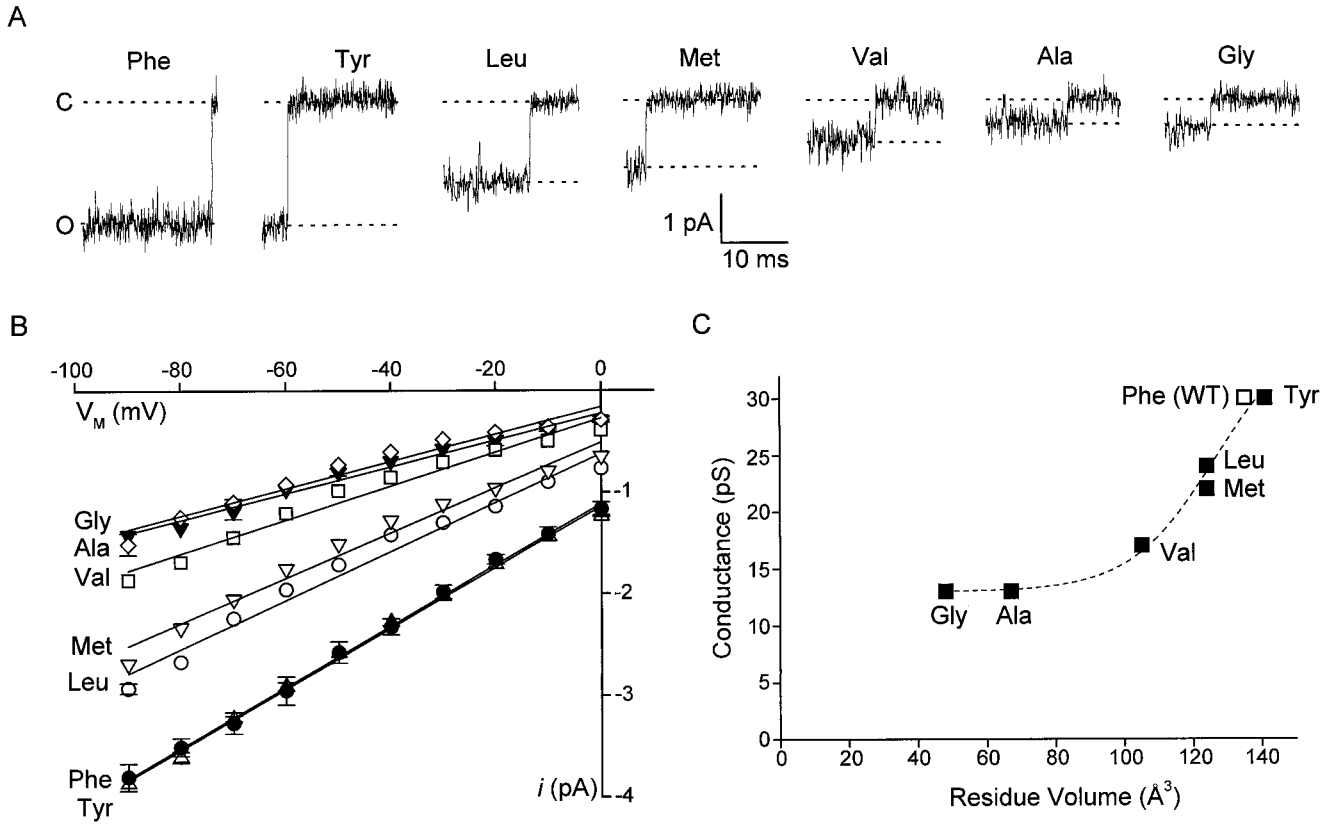

FIGURE 3 Influence of side-chain volume at the −1 position on unitary conductance in α_{1C} channels. (*A*) Single-channel records for wild-type $\alpha_{1C}{}^{FEG}$ and the mutant channels $\alpha_{1C}{}^{YEG}$, $\alpha_{1C}{}^{LEG}$, $\alpha_{1C}{}^{MEG}$, $\alpha_{1C}{}^{VEG}$, $\alpha_{1C}{}^{AEG}$, and $\alpha_{1C}{}^{GEG}$, recorded at a test potential of −40 mV. Inward currents were carried by 110 mM Ba^{2+} in the presence of 2 μM FPL 64176 to prolong channel open time. Holding potential, −80 mV. (*B*) Single-channel current-voltage relationships for the channels illustrated in *A*: $\alpha_{1C}{}^{FEG}$ (WT, ●; $n = 3$–6), $\alpha_{1C}{}^{YEG}$ (△; $n = 3$), $\alpha_{1C}{}^{LEG}$ (○; $n = 3$), $\alpha_{1C}{}^{MEG}$ (▽; $n = 3$), $\alpha_{1C}{}^{VEG}$ (□; $n = 3$), $\alpha_{1C}{}^{AEG}$ (◇; $n = 3$), and $\alpha_{1C}{}^{GEG}$ (▼; $n = 3$–5). (*C*) Single-channel conductance in 110 mM Ba^{2+} for wild-type and −1 position mutant channels plotted versus residue volume. Residue volumes were obtained from Creighton (1993).

The −1 position in α_{1C} and ion selectivity: binding affinity

Despite the lack of effect of the −1 position mutation upon selectivity as measured by reversal potentials, the apparent volume dependence of outward K^+ currents suggested that further investigation of the role of this position in selective ion permeation was warranted. We therefore probed the ion selectivity of the −1 position mutants, using measurement of block by external Cd^{2+} of Ba^{2+} current. Cd^{2+} ions compete with Ba^{2+} ions for high-affinity binding within the pore of Ca^{2+} channels (Kuo and Hess, 1993; Chow, 1991; Lansman et al., 1986), and thus the ability of the channel to bind Cd^{2+} provides an indication of the affinity of the pore for divalent ions, the basis of ion selectivity in these channels. Cd^{2+} dose-inhibition relationships for the −1 position mutants and the wild-type channel are illustrated in Fig. 4 *C*. The dose-inhibition data were well described by 1:1 binding functions, which yielded half-block concentrations (IC_{50}) as estimates of apparent binding affinity for Cd^{2+}. All of the mutants except $\alpha_{1C}{}^{YEG}$ had IC_{50} values higher than that of wild type, indicating a reduction in binding affinity for divalent cations in the mutants. The IC_{50} values for these mutants followed a general trend, shown in Fig. 4 *D*: the smaller the amino acid at the −1 position, the lower the apparent binding affinity. The dependence of IC_{50} upon residue volume is reminiscent of that seen for unitary conductance, although in that case, conductance decreased as residue volume decreased.

Effects of combined mutations at the 0 and −1 positions in α_{1C} and in α_{1A}

Apparent binding affinity of double mutants

Comparison of two previous studies (Kim et al., 1993; Yang et al., 1993) shows that substitution of the glutamate in motif III with glutamine (the $E_{III}Q$ mutation) has a much more profound impact on Cd^{2+} block of Ba^{2+} current in α_{1A} than in α_{1C}. Our finding that the amino acid at the −1 position in motif III influences Cd^{2+} binding led us to ask whether the nature of this neighboring amino acid determines the differential Cd^{2+} block of the $E_{III}Q$ mutants of α_{1C} and α_{1A}.

Fig. 5 illustrates the distinct effects of $E_{III}Q$ substitution upon Cd^{2+} block of whole-oocyte Ba^{2+} current in α_{1C} and α_{1A} channels. Wild-type α_{1C} and α_{1A} channels were virtually completely blocked by 30 μM Cd^{2+} (Fig. 5, *A* and *B*, *left*). The same concentration of Cd^{2+} blocked ~90% of the

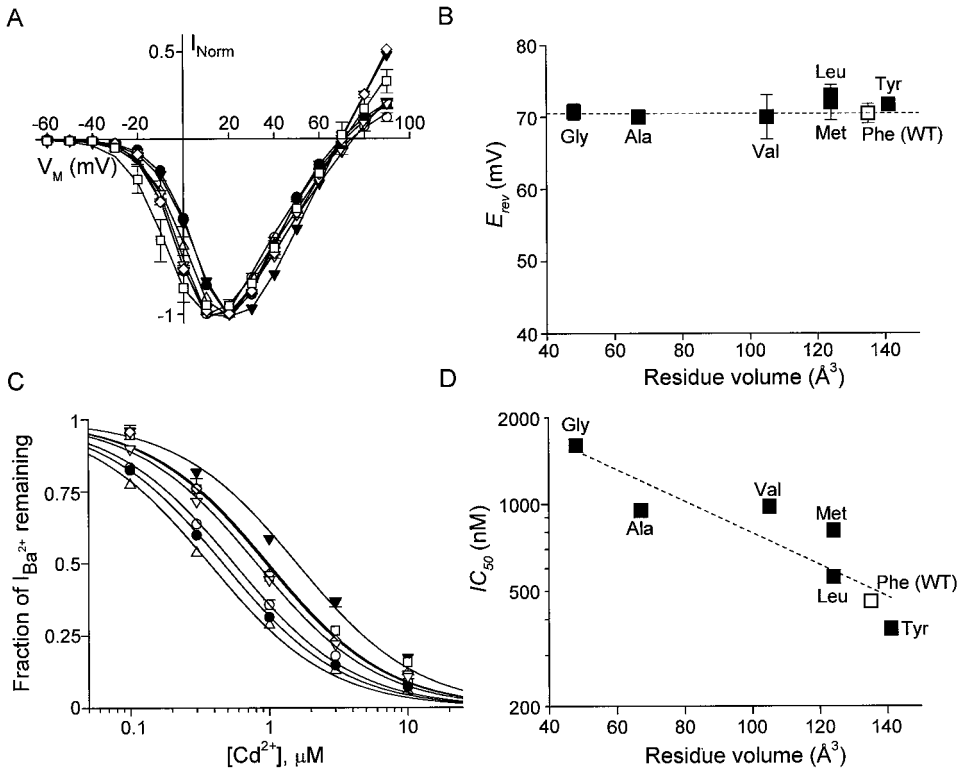

FIGURE 4 Ion selectivity of −1 position α_{1C} mutants. (*A*) Normalized, two-electrode voltage-clamp measurements of whole-oocyte peak current-voltage relationships for wild-type $\alpha_{1C}{}^{FEG}$ (●; $n = 4$) and the mutant channels $\alpha_{1C}{}^{YEG}$ (△; $n = 3$), $\alpha_{1C}{}^{LEG}$ (○; $n = 3$), $\alpha_{1C}{}^{MEG}$ (▽; $n = 4$), $\alpha_{1C}{}^{VEG}$ (□; $n = 4$), $\alpha_{1C}{}^{AEG}$ (◇; $n = 4$), and $\alpha_{1C}{}^{GEG}$ (▼; $n = 6$). Holding potential, −80 mV; 40 mM Ba^{2+} solution. (*B*) Plot of reversal potential versus residue volume at the −1 position. (*C*) Normalized peak Ba^{2+} current plotted against external Cd^{2+} concentration for wild-type $\alpha_{1C}{}^{FEG}$ and the −1 position mutant channels shown in *A*. Symbols represent the average of four to seven experiments for $\alpha_{1C}{}^{FEG}$ (WT), four experiments for $\alpha_{1C}{}^{GEG}$ and $\alpha_{1C}{}^{MEG}$, and three experiments for $\alpha_{1C}{}^{YEG}$, $\alpha_{1C}{}^{LEG}$, $\alpha_{1C}{}^{VEG}$, and $\alpha_{1C}{}^{AEG}$. Smooth curves represent best fits to the data of 1:1 binding functions. Holding potential, −80 mV; test potential, +20 mV; 40 mM Ba^{2+} solution. (*D*) Plot of IC_{50} for Cd^{2+} block of inward Ba^{2+} current versus residue volume at the −1 position.

Ba^{2+} current in the $E_{III}Q$ mutant of α_{1C}, $\alpha_{1C}{}^{FQG}$ (Fig. 5 *A*, *right*), but blocked only ~5% of Ba^{2+} current in the $E_{III}Q$ mutant of α_{1A}, $\alpha_{1A}{}^{GQG}$ (Fig. 5 *B*, *right*).

Dose-inhibition relationships for Cd^{2+} block of Ba^{2+} current in wild-type and $E_{III}Q$ mutant channels are illustrated in Fig. 6 *A* (*top*). Both kinds of wild-type channels

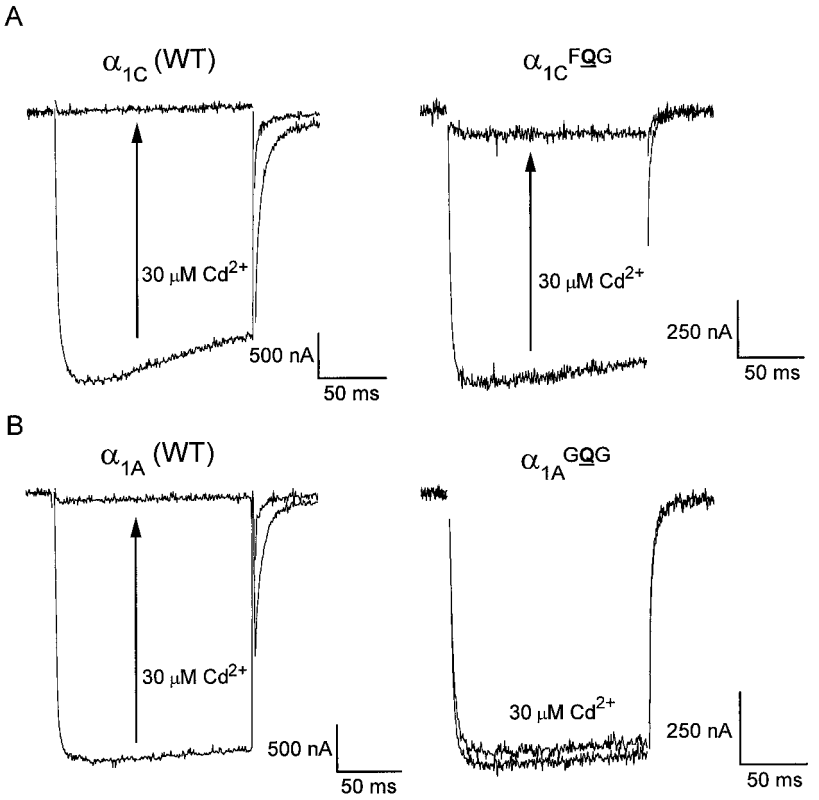

FIGURE 5 Cd^{2+} block of whole-oocyte Ba^{2+} currents in $\alpha_{1C}{}^{FEG}$ (WT) and $\alpha_{1A}{}^{GEG}$ (WT) and their corresponding $E_{III}Q$ mutants, $\alpha_{1C}{}^{FQG}$ and $\alpha_{1A}{}^{GQG}$. (*A*) Examples of block by 30 μM Cd^{2+} of whole-oocyte Ba^{2+} currents through $\alpha_{1C}{}^{FEG}$ (WT) and $\alpha_{1C}{}^{FQG}$ channels. Holding potential, −80 mV; test potential, +20 mV; 40 mM Ba^{2+} solution. (*B*) Examples of block by 30 μM Cd^{2+} of whole-oocyte Ba^{2+} currents through $\alpha_{1A}{}^{GEG}$ (WT) and $\alpha_{1A}{}^{GQG}$ channels. Holding potential, −80 mV; test potential, +20 mV; 40 mM Ba^{2+} solution.

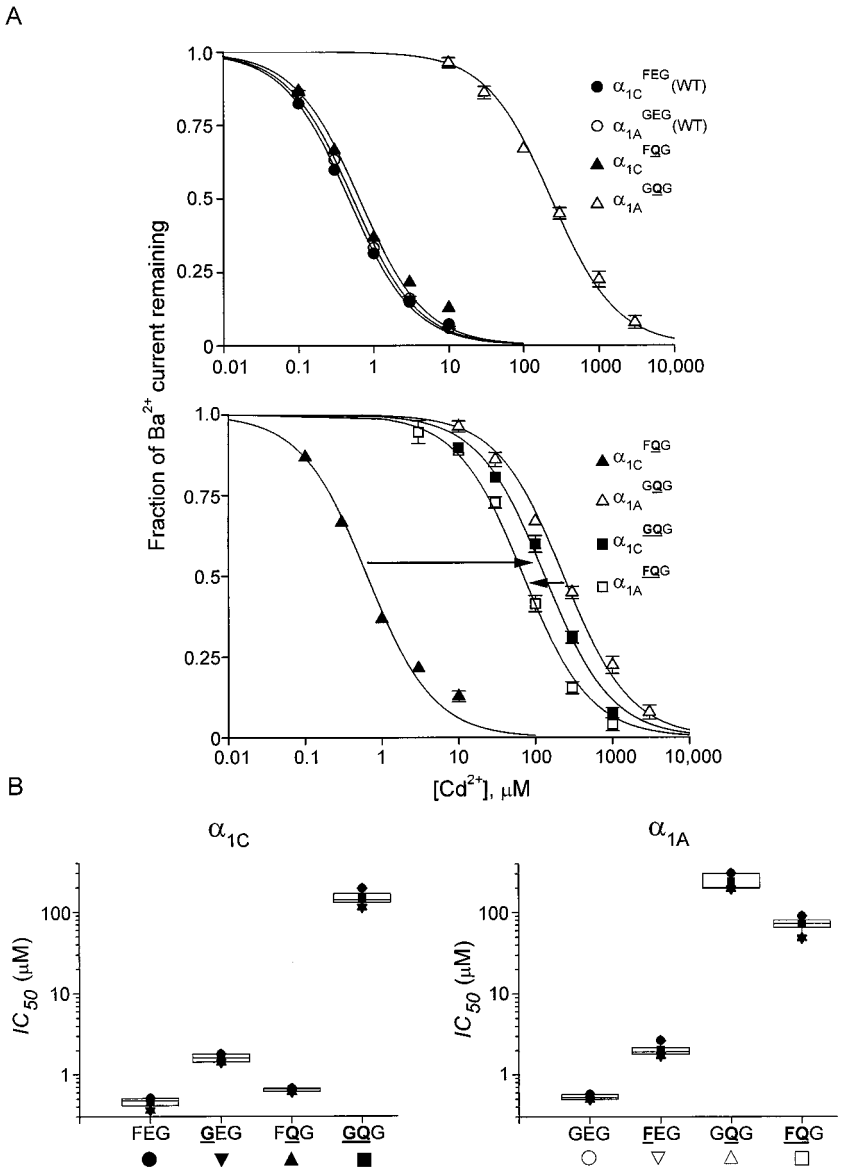

FIGURE 6 Concentration dependence of Cd^{2+} block of Ba^{2+} current through $E_{III}Q$ mutants and the influence of −1 position substitutions on Cd^{2+} block of $E_{III}Q$ mutants. (*A, top*) Fractional whole-oocyte Ba^{2+} current plotted against external Cd^{2+} concentration for α_{1C}^{FEG} (WT) and α_{1A}^{GEG} (WT) and their corresponding $E_{III}Q$ mutant channels, α_{1C}^{FQG} and α_{1A}^{GQG}. Symbols represent the average of four to seven experiments for α_{1C}^{FEG} (WT) and α_{1A}^{GEG} (WT), and four experiments each for α_{1C}^{FQG} and α_{1A}^{GQG}. Smooth curves represent best fits to the data of 1:1 binding functions. Holding potential, −80 mV; test potential, +20 mV; 40 mM Ba^{2+} solution. (*A, bottom*) Fractional whole-oocyte peak Ba^{2+} current plotted against external Cd^{2+} concentration for the $E_{III}Q$ mutant channels α_{1C}^{FQG} and α_{1A}^{GQG} and their corresponding double mutants α_{1C}^{GQG} and α_{1A}^{FQG}. Symbols represent the average of four experiments for α_{1C}^{FQG}, four experiments for α_{1A}^{GQG}, five experiments for α_{1C}^{GQG}, and two to six experiments for α_{1A}^{FQG}. Smooth curves represent best fits to the data of 1:1 binding functions. Holding potential, −80 mV; test potential, +20 mV; 40 mM Ba^{2+} solution. (*B*) Box plots summarizing IC_{50} values for Cd^{2+} block of whole-oocyte Ba^{2+} current in (*left*) wild-type and mutant α_{1C} channels and in (*right*) wild-type and mutant α_{1A} channels.

were very sensitive to Cd^{2+}, with IC_{50} values of 0.47 μM for α_{1C} and 0.53 μM for α_{1A}. The $E_{III}Q$ mutation in α_{1C} (α_{1C}^{FQG}) increased the IC_{50} by less than twofold, from 0.47 μM to 0.65 μM, whereas the $E_{III}Q$ mutation in α_{1A} (α_{1A}^{GQG}) had a much more profound effect on Cd^{2+} block, increasing the IC_{50} by more than 400-fold, from 0.53 μM to 232 μM.

To test the idea that the nature of the −1 neighbor in these two channels specifies, at least in part, differences in IC_{50} between the two $E_{III}Q$ mutants, we constructed and studied two double-mutant channels: α_{1C}^{GQG} and α_{1A}^{FQG}. Fig. 6 *A* (*bottom*) compares the dose-inhibition relationships for Cd^{2+} block of Ba^{2+} current in the double-mutant channels with those of the single $E_{III}Q$ mutant channels. Consistent with the hypothesis, substitution of glycine for phenylalanine in the $E_{III}Q$ mutant of α_{1C} increased the IC_{50} from 0.65 μM (α_{1C}^{FQG}) to 132 μM (α_{1C}^{GQG}; *rightward arrow*). Correspondingly, substitution of phenylalanine for glycine in the $E_{III}Q$ mutant of α_{1A} decreased the IC_{50} from 232 μM (α_{1A}^{GQG}) to 70 μM (α_{1A}^{FQG}; *leftward arrow*). The IC_{50} values for the wild-type and mutant channels are summarized in Fig. 6 *B*.

Reversal potential of double mutants

We also compared reversal potentials measured for the single $E_{III}Q$ mutations with those of the combined −1 position/$E_{III}Q$ mutants (double mutants). Fig. 7 *A* illustrates families of whole-oocyte Ba^{2+} currents recorded for wild type and the $E_{III}Q$ and double mutant α_{1C} and α_{1A} channels. The mutations shifted reversal potentials to less positive values: in contrast to the case for wild-type channels, at +60 mV, all four mutant channels (α_{1C}^{FQG}, α_{1C}^{GQG}, α_{1A}^{GQG}, and α_{1A}^{FQG}) exhibited large outward currents; at +40 mV, the two $E_{III}Q$ mutants possessing a glycine at the −1

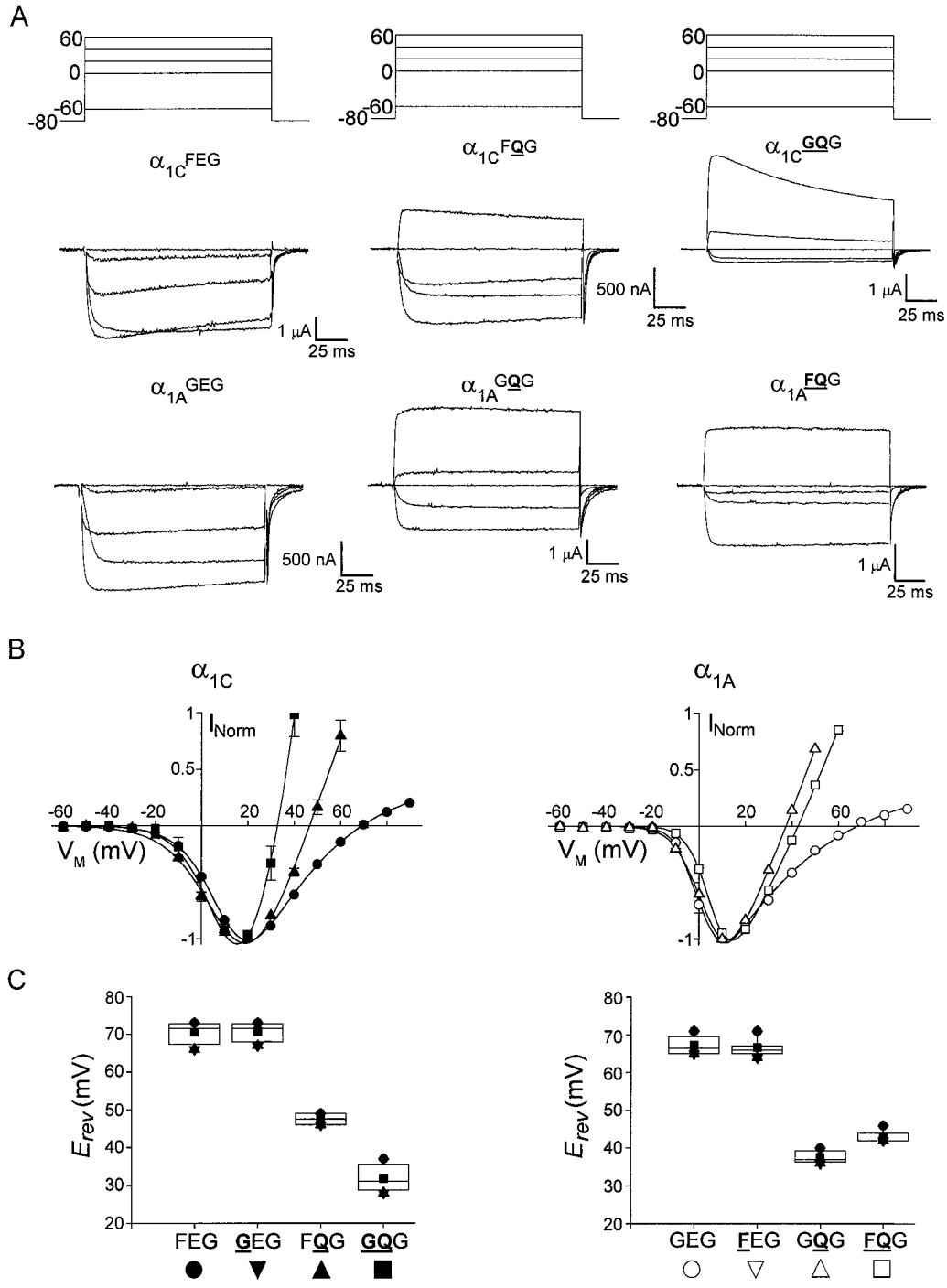

FIGURE 7 Reversal potential measurements for wild-type, $E_{III}Q$ mutant, and double mutant channels. (*A*) Families of whole-oocyte Ba^{2+} currents from wild-type and mutant α_{1C} and α_{1A} channels. The current records illustrated were obtained at −60, 0, +20, +40, and +60 mV. Holding potential, −80 mV; 40 mM Ba^{2+} solution. (*B*) Normalized and averaged current-voltage relationships for (*left*) α_{1C}^{FEG} (●; $n = 4$), α_{1C}^{FQG} (▲; $n = 6$), and α_{1C}^{GQG} (■; $n = 6$); (*right*) wild-type channel α_{1A}^{GEG} (○; $n = 7$), α_{1A}^{GQG} (△; $n = 4$), and α_{1A}^{FQG} (□; $n = 6$). Holding potential, −80 mV; 40 mM Ba^{2+} solution. (*C*) Box plot summarizing reversal potential measurements for wild-type and mutant (*left*) α_{1C} and (*right*) α_{1A} channels.

position (α_{1C}^{GQG} and α_{1A}^{GQG}) also exhibited outward currents.

Normalized, averaged peak current-voltage relationships are illustrated in Fig. 7 *B* for wild-type and mutant forms of α_{1C} (*left*) and α_{1A} (*right*) channels. Inward Ba^{2+} currents carried by the two wild-type channels (α_{1C} and α_{1A}) reversed near +70 mV, with small outward currents (carried by K^+) observed above the reversal potential. All four $E_{III}Q$ mutant channels (α_{1C}^{FQG}, α_{1C}^{GQG}, α_{1A}^{GQG}, and α_{1A}^{FQG}) exhibited much less positive reversal potentials, in the range of ~ +30 to +45 mV, indicating large reductions in selectivity for Ba^{2+} over K^+ in the $E_{III}Q$ mutants. Reversal

potential measurements for wild-type channels and for $E_{III}Q$, −1 position, and double-mutant channels are summarized in the box plots in Fig. 7 *C*. The summary shows that, for α_{1C} (*left*) and α_{1A} (*right*), although substitution at the −1 position alone has little bearing upon reversal potential, combining substitution at this position with the $E_{III}Q$ mutation does influence reversal potential.

DISCUSSION

As a tactic to help understand how high flux through the selectivity locus is achieved in voltage-gated Ca^{2+} channels, we have begun to investigate how amino acids neighboring the EEEE locus influence various features of selective Ca^{2+} transport through the pore. The results of this work provide the first identification of an amino acid neighbor involved in tuning EEEE locus function. Specifically, the amino acid at the −1 position in motif III influences ion selectivity in both Ca^{2+} channel subfamily exemplars studied, α_{1C} and α_{1A}, and the amino acid at this position also partly controls unitary conductance in α_{1C} although not in α_{1A} channels. Our finding of a relationship in α_{1C} between unitary conductance and side-chain volume at the −1 position provides insight into the mechanism of interaction between EEEE locus and neighbors.

Ion binding affinity is a sensitive measure of the effects of mutations on ion selectivity

We used two paradigms to measure ion selectivity in Ca^{2+} channels: reversal potential, which yields the permeability of Ba^{2+} relative to K^+ (P_{Ba}/P_K), and apparent binding affinity (IC_{50}), which yields the free energy of divalent cation binding in the pore. Previous work had shown that the $E_{III}Q$ substitution shifts reversal to a less positive potential for both α_{1C} and α_{1A} channels. We have found, in contrast, that reversal was completely insensitive to amino acid substitution at the −1 neighbor position in either of these channels. The conclusion is that substitution for E_{III}, but not for the −1 neighbor, alters pore affinity for Ba^{2+} over K^+. Does this mean that ion selectivity is unaffected by −1 position mutagenesis?

As shown previously, $E_{III}Q$ mutations in α_{1C} and α_{1A} increased the IC_{50} for Cd^{2+} block of Ba^{2+} current, paralleling their effects on reversal potentials (Kim et al., 1993; Yang et al., 1993). Moreover, all of the −1 position mutations that we made in α_{1C} and in α_{1A} channels also compromised Cd^{2+} block of Ba^{2+} current, as indicated by the increased IC_{50} values for Cd^{2+} block in all mutants. Indeed, for α_{1C}, the F→G mutation at the −1 position had a larger effect than did the $E_{III}Q$ mutation (Fig. 6 *B*). Thus −1 position substitutions do influence ion selectivity, and to a degree not necessarily less significant than that arising from single EEEE locus substitutions. An adjunct conclusion is that measurement of the IC_{50} detected effects of −1 substitution that were missed by reversal potential measurement. We suppose that the seemingly higher sensitivity of the IC_{50} measurements as compared to reversal potential measurements reflects largely the differing experimental conditions used to obtain these two parameters. IC_{50} measures pore preference for Cd^{2+} over Ba^{2+}, with both of these ions inwardly directed through the pore. In counterpoint, E_{rev} measures pore preference for inwardly directed Ba^{2+} over outwardly directed K^+, with the affinity for K^+ being very low compared to that for Ba^{2+}.

Double mutations reveal −1 neighbor interaction with the EEEE locus

Although E_{rev} was insensitive to the −1 neighbor position mutation alone, E_{rev} was strongly affected by combining mutations at the −1 position with the $E_{III}Q$ mutation. For the α_{1C} double mutant, E_{rev} was shifted by about −40 mV, while in the α_{1A} double mutant E_{rev} was shifted by about −25 mV. Comparison of the single $E_{III}Q$ mutant channels with the doubles reveals an interesting point: for α_{1C}, E_{rev} was less affected by the single $E_{III}Q$ mutation than by double mutation, whereas the reverse was true for α_{1A}. Ignoring whether particular constructs are wild type or single or double mutants and instead comparing constructs with similar sequences, Fig. 8 *A* (*upper panels*) shows that the sequence-dependent pattern of selectivity for Ba^{2+} over K^+ is very similar between α_{1C} and α_{1A}. As alluded to above, whether the −1 neighbor is a phenylalanine or a glycine is of no consequence for the P_{Ba}/P_K of α_{1C} and of α_{1A} channels, but on an $E_{III}Q$ background, glycine in the −1 neighbor position reduces P_{Ba}/P_K more than does phenylalanine in this position for both kinds of channels. One or more characteristics of these amino acids, including side-chain volume and a variety of chemical properties, might account for this observation, but making such an assessment will require at least an analysis of a series of systematic −1 position mutations on an $E_{III}Q$ background.

The fact that P_{Ba}/P_K is determined not by the numbers of mutations made, but rather by the amino acid sequence alone, helps to establish the usefulness of our mutant constructs and the significance of our results in a general sense. That P_{Ba}/P_K correlates with amino acid sequence independently of parent channel type (α_{1C} or α_{1A}) indicates that the mutations did not generally disrupt pore structure. Mutational alteration of pore function is therefore most likely attributable to small-scale changes in pore structure, according to the differing properties of the substituted amino acids, and not to more far-reaching effects on protein structure.

Like reversal potential, Cd^{2+} binding affinity in the double mutants was also dependent upon the identity of the −1 position neighbor. Fig. 8 *A* (*lower panels*) summarizes free energies of Cd^{2+} binding for both α_{1C} and α_{1A} constructs, as calculated from the apparent binding affinities described in Fig. 6. As in the upper panels of Fig. 8, the data are again presented in a manner that facilitates comparison of channels with similar sequences, rather than with similar num-

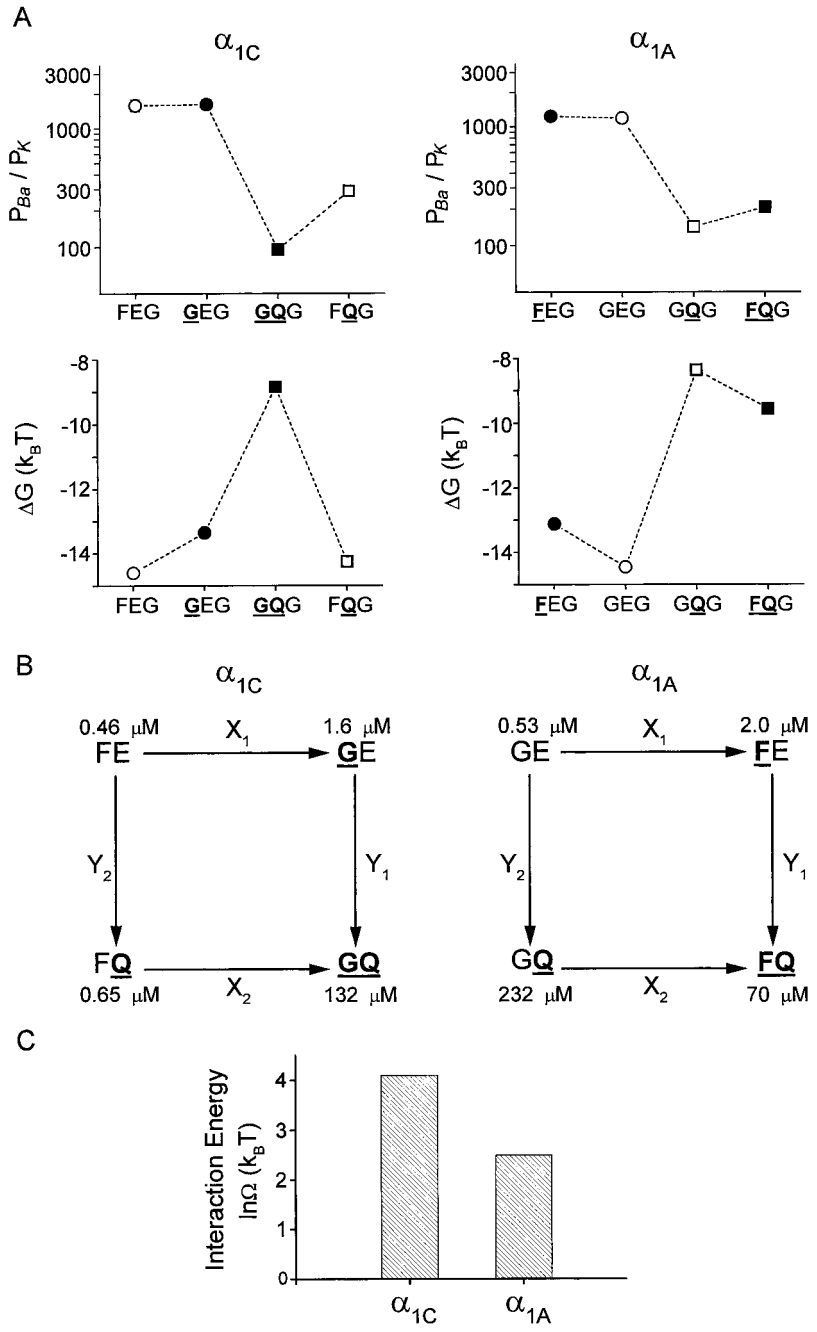

FIGURE 8 Summary of ion selectivity properties and mutant cycle analysis for α_{1C} and α_{1A} constructs. (*A, top*) Permeability ratios (P_{Ba}/P_K) displayed versus pore sequence for α_{1C} and α_{1A} constructs. ○ = wild-type, □ = $E_{III}Q$ mutant, ● = −1 position mutant, ■ = double mutant. (*A, bottom*) Free energy of Cd^{2+} binding (ΔG) displayed versus pore sequence for α_{1C} and α_{1A} constructs. (*B*) Thermodynamic mutant cycles used to examine the interaction between E_{III} and the −1 position amino acid for α_{1C} and α_{1A} channels. Each step around the mutant cycle represents a single mutational difference, and the corresponding fold change in Cd^{2+} binding affinity is symbolized by the uppercase labels (X_1, X_2 for the −1 position mutation; Y_1, Y_2 for the $E_{III}Q$ mutation). For example, $X_1 = K'_D(\text{mut.1})/K'_D(\text{wt})$, where K'_D is the apparent equilibrium dissociation constant, mut.1 is the −1 position mutation with E_{III} intact, and wt indicates the wild-type channel. Measured IC_{50} values for Cd^{2+} block have been used as approximations of the requisite K'_D values. The strength of interaction between residues is characterized by the coupling coefficient Ω, defined as

$$\Omega = \frac{X_1}{X_2} = \frac{Y_2}{Y_1} = \frac{IC_{50}(\text{mut.1}) \cdot IC_{50}(\text{mut.2})}{IC_{50}(\text{wt}) \cdot IC_{50}(\text{mut.1 + mut.2})}$$

The coupling energy for the pair of mutations is given by $\Delta G = k_B T \cdot \ln(\Omega)$, with $\Omega = 1$ (or $\Delta G = 0$) indicating that the amino acids of the pair do not interact in a cooperative way to bind Cd^{2+}. A nonzero coupling energy represents the degree of nonadditivity, or cooperativity, in the energetic effects of the single mutations. (*C*) Free energy of interaction between E_{III} and the −1 position amino acid in α_{1C} and in α_{1A}, calculated as the natural logarithm of the coupling parameter (Ω) obtained from the thermodynamic mutant cycle analysis.

bers of mutations. Cd^{2+} binding energy was weakest for the combination of the $E_{III}Q$ mutation with a glycine at the -1 position, regardless of whether the glycine was naturally occurring or introduced by mutagenesis. The estimated Cd^{2+} binding energies (ΔG) for the GQG sequence in α_{1C} and in α_{1A} channels, respectively, were -8.9 and $-8.4k_BT$. Although binding energies for α_{1C} and α_{1A} were approximately similar for this sequence, this was not the case for the other three pore sequences investigated. The largest difference between α_{1C} and α_{1A} channels was observed for the FQG sequence. Although for both α_{1C} and α_{1A} channels the binding energies associated with the FQG sequences were stronger than those for GQG, in α_{1C}, the Cd^{2+} binding energy measured for the FQG sequence was almost the same as that for FEG, but in α_{1A}, FQG differed very significantly from FEG, by $\sim 5k_BT$. When the effects of -1 position identity were compared when E_{III} was intact, α_{1C} and α_{1A} differed modestly but significantly from one another in binding energy, by $1.5k_BT$ for FEG and by $1.2k_BT$ for GEG.

The discrete changes in Cd^{2+} binding energy resulting from stepwise mutation at the -1 position, E_{III}, and both of these positions together represents a thermodynamic cycle or mutant cycle. Analysis of mutant cycles was developed to examine interacting amino acid residues within proteins (Horovitz and Fersht, 1990; Carter et al., 1984) and has also been used to identify residues involved in protein-protein interaction (Schreiber and Fersht, 1995). For K^+ channels and the pore-blocking peptide charybdotoxin, interacting toxin-channel amino acid pairs have been identified by mutant cycle analysis (Ranganathan et al., 1996; Hidalgo and MacKinnon, 1995). In Ca^{2+} channels, mutant cycles have been used to quantitate the interplay among EEEE locus glutamates in the binding of divalent cations (Ellinor et al., 1995). Here we extend the analysis of interaction among Ca^{2+} channel pore residues to include non-EEEE locus amino acids, specifically the -1 position in motif III. The simple principle underlying this version of mutant cycle analysis is this: if two residues interact with one another in binding the same ligand, which in our case is Cd^{2+}, then mutating one or the other of these positions will not only directly modify that position's participation in ligand binding; it will also influence the interaction of the nonmutated position with the ligand.

Fig. 8 *B* illustrates the mutant cycles for α_{1C} and for α_{1A} channels. For α_{1C}, the F→G mutation with E_{III} intact increased IC_{50} by 3.5-fold (X_1), whereas the same F→G mutation on an $E_{III}Q$ background increased the IC_{50} by 200-fold (X_2). The $E_{III}Q$ mutation with the F at the -1 position intact increased the IC_{50} by 1.4-fold (Y_1), whereas the $E_{III}Q$ mutation on an F→G background increased the IC_{50} by 83-fold (Y_2). Likewise for α_{1A}, the G→F mutation with E_{III} intact increased the IC_{50} by 3.8-fold, whereas the same G→F mutation on an $E_{III}Q$ background changed the IC_{50} by 0.3-fold. The $E_{III}Q$ mutation with the G at the -1 position intact increased the IC_{50} by 438-fold, whereas the same $E_{III}Q$ mutation on a G→F background increased the IC_{50} by only 35-fold. For both parent channel types, that the effect of -1 position mutagenesis strongly depends upon the identity of the residue at the 0 position and, in a complementary fashion, that the effect of 0 position mutagenesis strongly depends upon the identity of the residue at the -1 position, suggest a significant coupling between the -1 and 0 positions in Cd^{2+} binding. The coupling energies for -1 position/0 position interaction were calculated as $4.1k_BT$ and $2.4\ k_BT$ for α_{1C} and α_{1A}, respectively (Fig. 8 *C*; see legend). Both of these coupling energies are large, comparing favorably to the strongest coupling energies measured for amino acid pairs specifically involved in charybdotoxin binding to K^+ channels (Ranganathan et al., 1996). Indeed, coupling between the -1 and 0 positions is stronger than coupling measured previously for any of the six pairings of glutamates in the EEEE locus itself (range: $0.4–1.4k_BT$; Ellinor et al., 1995). Strong interactions between the -1 and 0 positions therefore suggest that the -1 position plays a comparatively important role in EEEE locus function via interaction with E_{III}. Alternatively, the large coupling energies arise from a noninteresting source, nonspecific mutational disruption of pore structure. This possibility seems unlikely because 1) the mutations did not prevent high ion flux through the pore and 2) P_{Ba}/P_K obeyed pore sequence, independent of the number of mutations made, across α_{1C} and α_{1A} (see above). Comparing the role of the -1 position in α_{1C} with its role in α_{1A} shows, in parallel with the results for unitary conductance, that the -1 position couples more strongly with E_{III} in α_{1C} than it does in α_{1A}.

Difference between α_{1C} and α_{1A} in the -1 position function

The incongruences in Cd^{2+} binding energies noted in the preceding section between the four pore-lining sequences tested in α_{1C} and α_{1A}, with the probable exception of the GQG sequence, were energetically significant. For α_{1C} and α_{1A} channels, respectively, Cd^{2+} binding energies were -14.6 and $-13.1k_BT$ for FEG, $-13.3k_BT$ and $-14.5k_BT$ for GEG, and $-14.3k_BT$ and $-9.6k_BT$ for FQG. For these three sequences, the binding energies differed between α_{1C} and α_{1A} backgrounds by (absolute value) $1.5k_BT$, $1.2k_BT$, and $4.7k_BT$, which translate to 3.7, 3.0, and 11.7 kJ/mol. These energy differences are comparable in size to close-approach electrostatic interactions between amino acid residues and indicate that the context, whether α_{1C} or α_{1A}, clearly matters. Further evidence that α_{1C} and α_{1A} differ in the degree to which the -1 position is involved in regulating pore function includes the following two observations: for the complementary F→G and G→F mutations in α_{1C} and α_{1A}, neither unitary conductance (Fig. 2) nor outward current magnitude (Fig. 1) was reciprocally modified (Fig. 2). That individual pore-lining amino acids differ in function between α_{1C} and α_{1A} is not surprising, because one of the experimental observations that spurred our investigation of the -1 position was that the $E_{III}Q$ mutation was very different (310-fold, relative to each wild-type channel) in

the degree to which it right-shifted IC_{50} in the two parent channel types. Thus although the background was not important for all pore parameters investigated (for example, P_{Ba}/P_K), differences in channel structure outside of the small region that we have investigated determine many features of channel type-specific pore properties. Previous work on α_{1A} channels points to a candidate structural difference in motif IV, which plays a relatively more significant role in the unitary conductance of α_{1A} than does motif III (Yatani et al., 1994b). In the skeletal muscle L-type Ca^{2+} channel α_{1S}, a phenylalanine is present at the -1 position (Table 1), and yet this channel has a low unitary conductance of ~15 pS in 110 mM Ba^{2+} (Dirksen and Beam, 1995). The origin of this difference in unitary conductance between wild-type α_{1C} and α_{1S} channels has been narrowed down to the P-region of motif I (Dirksen et al., 1997). Combining work by others on α_{1A} and α_{1S} channels with our work here suggests that multiple channel structural elements may act in concert to govern unitary conductance in Ca^{2+} channels and that the relative contributions of these structural elements may differ across channel types. From the point of view of cell physiology, it is possible that various structural elements are involved, in a channel type-specific manner, in differentially tuning interactions between the EEEE locus glutamates and neighboring residues to allow distinct unitary conductances while preserving high selectivity for Ca^{2+}.

A clue regarding the mechanism of interaction between −1 neighbors and the EEEE locus

Many, but not all, single mutations made in the EEEE locus of α_{1C} have previously been found to decrease unitary Ba^{2+} current amplitude (Parent and Gopalakrishnan, 1995). The reduction in unitary Ba^{2+} current produced by a non-EEEE locus mutation in α_{1C}, the F→G substitution at the -1 position in motif III, was about as large as that found for the most severe of the single mutations in the EEEE locus. Although the complementary G→F mutation in α_{1A} had much less effect on unitary conductance, the large effect of -1 position substitution in α_{1C} led us to try to understand the structural basis of the observation in this channel type. Phenylalanine and glycine, the wild-type and first -1 position substitution that we studied, differ from one another in a variety of ways. Phenylalanine is much larger than glycine, is aromatic rather than aliphatic, has a chiral α-carbon whereas glycine does not, and is significantly more hydrophobic than glycine (Creighton, 1993). Phenylalanine, by virtue of its aromatic nature, can also interact favorably with permeant metal cations through an electrostatic cation-π orbital mechanism (Kumpfe and Dougherty, 1993; Heginbotham and MacKinnon, 1992). To try to understand the physical and chemical nature of the interaction between the -1 position residue and E_{III}, we tested a variety of additional uncharged amino acid substitutions at the -1 position. For the substitutions tested, we found a clear, nonlinear relationship between unitary slope conductance (γ) and residue volume (Fig. 3 *C*). We also found a linear relationship between IC_{50} for Cd^{2+} block of Ba^{2+} current and residue volume (Fig. 4 *D*). Outward currents, which were carried by exiting K^+ ions in the whole-oocyte experiments, also varied in a systematic manner with residue volume (Fig. 4 *A*), likely as a result of altered unitary conductance. In contrast, reversal potential, which was unchanged by the F→G substitution, was insensitive to the other four mutations investigated (Fig. 4 *B*) as well, fitting with the notion that this measure is simply less sensitive to pore mutations.

Interestingly, the volume-related trends for γ and IC_{50} have opposite slopes, so that γ increases as residue volume increases but IC_{50} decreases with increasing volume. Since γ exclusively reflects Ba^{2+} interactions in the pore whereas IC_{50} reflects largely Cd^{2+} interactions, and both of these ions enter from the extracellular solution and then exit into the cytosol, one interpretation of these opposing trends is that increasing amino acid side-chain volume increases Ba^{2+} flux but decreases Cd^{2+} flux. Such differences in interaction with the pore might arise from differences in the coordination structure of these metal ions, an issue that could be resolved by testing other divalent ions, particularly Ca^{2+}, which has a structure similar to that of Ba^{2+} (Falke et al., 1994).

The strong relationships between residue volume and both γ and IC_{50} provide a clue regarding the mechanism of interaction between the natural -1 neighbor and E_{III}, at least in the α_{1C} channel. The most economical interpretation of the volume dependencies for γ and IC_{50} is a steric one: it is possible that the wild-type pattern of alternating small- and large-volume side chains at the -1 and $+1$ positions causes a splaying of the EEEE-locus ring structure, providing the ability of the EEEE locus to simultaneously interact with two Ca^{2+} ions. However, although residue volume was the simple parameter that we chose to plot in Figs. 3 and 4, trends similar to those obtained using residue volume were generated for both γ and IC_{50} when plotted versus side-chain surface area, and less well, versus residue hydrophobicity (not shown). Moreover, although volume might be the key factor in the mutational effects, the specific consequence of alteration of this characteristic (volume) on pore function is not necessarily straightforward. For example, decreasing the molecular volume of solvent increases glutamate carboxylate ionizability (Creighton, 1993), and because the "solvent" in the vicinity of the EEEE locus glutamates includes the neighboring amino acids, residue volume could conceivably modify pK_a's within the EEEE locus. The carboxylates of the EEEE locus side chains are obvious candidates for such modification, but it is unclear that they in fact project into the pore (Chen et al., 1997). Alternatively, the carbonyl oxygens of the glutamate α-carbons may project into the pore and bind permeant metal ions, as is the case in a bacterial K^+ channel (Doyle et al., 1998). A clear answer to the question of whether glutamate side chains project into the pore would be useful at this point.

We thank Tsutomu Tanabe, Veit Flockerzi, and Franz Hoffman for gifts of α_{1A}, α_{1C}, $\alpha_2\delta$, and β_{2b} subunit cDNAs.

This work was supported by grant NS35245 from the National Institutes of Health (WAS) and by a fellowship from the American Heart Association, Colorado and Wyoming Affiliate (AVW).

REFERENCES

Almers, W., and E. W. McCleskey. 1984. Non-selective conductance in calcium channels of frog muscle: calcium selectivity in a single-file pore. *J. Physiol. (Lond.).* 353:585–608.

Almers, W., E. W. McCleskey, and P. T. Palade. 1984. A non-selective cation conductance in frog muscle membrane blocked by micromolar external calcium ions. *J. Physiol. (Lond.).* 353:565–583.

Bahinski, A., A. Yatani, G. Mikala, S. Tang, S. Yamamoto, and A. Schwartz. 1997. Charged amino acids near the pore entrance influence ion-conduction of a human L-type cardiac calcium channel. *Mol. Cell. Biochem.* 166:125–134.

Barrish, M. E. 1983. A transient calcium-dependent chloride current in the immature *Xenopus* oocyte. *J. Physiol. (Lond.).* 342:309–325.

Blinks, J. R., W. G. Wier, P. Hess, and F. G. Prendergast. 1982. Measurement of Ca^{2+} concentrations in living cells. *Prog. Biophys. Mol. Biol.* 40:1–114.

Campbell, D. L., W. R. Giles, J. R. Hume, D. Noble, and E. F. Shibata. 1988. Reversal potential of the calcium current in bull-frog atrial myocytes. *J. Physiol. (Lond.).* 403:267–286.

Carter, P. J., G. Winter, A. J. Wilkison, and A. R. Fersht. 1984. The use of double mutants to detect structural changes in the active site of the tyrosyl-tRNA synthetase. *Cell.* 38:835–840.

Chen, X. H., I. Bezprozvanny, and R. W. Tsien. 1997. Molecular basis of proton block of L-type Ca^{2+} channels. *J. Gen. Physiol.* 108:363–374.

Chow, R. H. 1991. Cadmium block of squid calcium currents. Macroscopic data and a kinetic model. *J. Gen. Physiol.* 98:751–770.

Creighton, T. E. 1993. Proteins: Structures and Molecular Properties. W. H. Freeman and Company, New York.

Dirksen, R. T., and K. G. Beam. 1995. Single calcium channel behavior in native skeletal muscle. *J. Gen. Physiol.* 105:227–247.

Dirksen, R. T., J. Nakai, A. Gonzalez, K. Imoto, and K. G. Beam. 1997. The S5–S6 linker of repeat I is a critical determinant of L-type Ca^{2+} channel conductance. *Biophys. J.* 73:1402–1409.

Doyle, D. A., J. M. Cabral, R. A. Pfuetzner, A. Kuo, J. M. Gulbis, S. L. Cohen, B. T. Chait, and R. MacKinnon. 1998. The structure of the potassium channel: molecular basis of K^+ conduction and selectivity. *Science.* 280:69–77.

Ellinor, P. T., J. Yang, W. A. Sather, J. F. Zhang, and R. W. Tsien. 1995. Ca^{2+} channel selectivity at a single locus for high-affinity Ca^{2+} interactions. *Neuron.* 15:1121–1132.

Falke, J. J., S. K. Drake, A. L. Hazard, and O. B. Peersen. 1994. Molecular tuning of ion binding to calcium signaling proteins. *Q. Rev. Biophys.* 27:219–290.

Heginbotham, L., and R. MacKinnon. 1992. The aromatic binding site for tetraethylammonium ion on potassium channels. *Neuron.* 8:483–491.

Hess, P., J. B. Lansman, and R. W. Tsien. 1986. Calcium channel selectivity for divalent and monovalent cations. Voltage and concentration dependence of single channel current in ventricular heart cells. *J. Gen. Physiol.* 88:293–319.

Hess, P., and R. W. Tsien. 1984. Mechanism of ion permeation through calcium channels. *Nature.* 309:453–456.

Hidalgo, P., and R. MacKinnon. 1995. Revealing the architecture of a K channel pore through mutant cycles with a peptide inhibitor. *Science.* 268:307–310.

Horovitz, A., and A. R. Fersht. 1990. Strategy for analysing the cooperativity of intramolecular interactions in peptides and proteins. *J. Mol. Biol.* 214:613–617.

Hullin, R., D. Singer-Lahat, M. Freichel, M. Biel, N. Dascal, F. Hofmann, and V. Flockerzi. 1992. Calcium channel beta subunit heterogeneity: functional expression of cloned cDNA from heart aorta and brain. *EMBO J.* 11:885–890.

Kim, M. S., T. Morii, L. X. Sun, K. Imoto, and Y. Mori. 1993. Structural determinants of ion selectivity in brain calcium channel. *FEBS Lett.* 318:145–148.

Kostyuk, P. G., S. L. Mironov, and Y. M. Shuba. 1983. Two ion-selecting filters in the calcium channel of the somatic membrane of mollusc neurons. *J. Membr. Biol.* 76:83–93.

Kumpfe, R. A., and D. A. Dougherty. 1993. A mechanism for ion selectivity in potassium channels: computational studies of cation-pi interactions. *Science.* 261:1708–1710.

Kuo, C. C., and P. Hess. 1993. Ion permeation through the L-type Ca^{2+} channel in rat phaeochromocytoma cells: two sets of ion binding sites in the pore. *J. Physiol. (Lond.).* 466:629–655.

Lansman, J. B., P. Hess, and R. W. Tsien. 1986. Blockade of current through single calcium channels by Cd^{2+}, Mg^{2+}, and Ca^{2+}. Voltage and concentration dependence of calcium entry into the pore. *J. Gen. Physiol.* 88:321–347.

Liman, E. R., J. Tytgat, and P. Hess. 1992. Subunit stoichiometry of a mammalian K^+ channel determined by construction of multimeric cDNAs. *Neuron.* 9:861–871.

McCleskey, E. W. 1999. Calcium channel permeation: a field in flux. *J. Gen. Physiol.* 113:765–772.

Mikala, G., A. Bahinski, A. Yatani, S. Tang, and A. Schwartz. 1993. Differential contribution by conserved glutamate residues to an ion-selectivity site in the L-type Ca^{2+} channel pore. *FEBS Lett.* 335: 265–269.

Mikami, A., K. Imoto, T. Tanabe, T. Niidome, Y. Mori, H. Takeshima, S. Narumiya, and S. Numa. 1989. Primary structure and functional expression of the cardiac dihydropyridine-sensitive calcium channel. *Nature.* 340:230–233.

Mori, Y., T. Friedrich, M.-S. Kim, A. Mikami, J. Nakai, P. Ruth, E. Bosse, F. Hofmann, V. Flockerzi, T. Furuichi, K. Mikoshiba, K. Imoto, T. Tanabe, and S. Numa. 1991. Primary structure and functional expression from complimentary DNA of a brain calcium channel. *Nature.* 350: 398–402.

Nonner, W., and B. Eisenberg. 1998. Ion permeation and glutamate residues linked by Poisson-Nernst-Planck theory in L-type calcium channels. *Biophys. J.* 75:1287–1305.

Parent, L., and M. Gopalakrishnan. 1995. Glutamate substitution in repeat IV alters divalent and monovalent cation permeation in the heart Ca^{2+} channel. *Biophys. J.* 69:1801–1813.

Ranganathan, R., J. H. Lewis, and R. MacKinnon. 1996. Spatial localization of the K^+ channel selectivity filter by mutant cycle-based structure analysis. *Neuron.* 16:131–139.

Robinson, R. A., and R. H. Stokes. 1959. Electrolyte Solutions. Butterworths, London.

Schreiber, G., and A. R. Fersht. 1995. Energetics of protein-protein interactions: analysis of the Barnase-Barstar interface by single mutations and double mutant cycles. *J. Mol. Biol.* 248:478–486.

Tang, S., G. Mikala, A. Bahinski, A. Yatani, G. Varadi, and A. Schwartz. 1993. Molecular localization of ion selectivity sites within the pore of a human L-type cardiac calcium channel. *J. Biol. Chem.* 268: 13026–13029.

Yang, J., P. T. Ellinor, W. A. Sather, J. F. Zhang, and R. W. Tsien. 1993. Molecular determinants of Ca^{2+} selectivity and ion permeation in L-type Ca^{2+} channels. *Nature.* 366:158–161.

Yatani, A., A. Bahinski, G. Mikala, S. Yamamoto, and A. Schwartz. 1994a. Single amino acid substitutions within the ion permeation pathway alter single-channel conductance of the human L-type cardiac Ca^{2+} channel. *Circ. Res.* 75:315–323.

Yatani, A., A. Bahinski, M. Wakamori, S. Tang, Y. Mori, T. Kobayashi, and A. Schwartz. 1994b. Alteration of channel characteristics by exchange of pore-forming regions between two structurally related Ca^{2+} channels. *Mol. Cell. Biochem.* 140:93–102.